Enhanced synaptic characteristics of electrolyte-gated oxide transistor enabled by optimizing interface states at the oxide semiconductor/electrolyte interface

Yan Li[a], Youbin Chen[b], Li Zhang[a], Shilong Ju[c], Ruihua Wang[a], Xiao Fu[d], Chuyi Fan[a], Xianzhe Liu[a,] *, Kuankuan Lu[f], Tian Qiu[e], Honglong Ning[d], Aiping Huang[a,] *, Jianyi Luo[a,] *

[a] Research Center of Flexible Sensing Materials and Devices, School of Applied Physics and Materials, Wuyi University, Jiangmen, 529020, China.
[b] School of Electrical and Electronic Engineering, Newcastle University, Newcastle upon Tyne NE1 7RU, United Kingdom.
[c] School of Computer Science and Engineering, Sichuan University of Science and Engineering, Zigong, 643002, China.
[d] Institute of Polymer Optoelectronic Materials and Devices, State Key Laboratory of Luminescent Materials and Devices, South China University of Technology, Guangzhou, 510640, China.
[e] School of Electronics and Information Engineering, Wuyi University, Jiangmen, 529020, China.
[f] Omat Advanced Materials (Guangdong) Co., Ltd., Shaoguan, 512029, China.
*Corresponding Author: liuxianzhe@wyu.edu.cn, flyinghap@163.com, luojiany@mail3.sysu.edu.cn

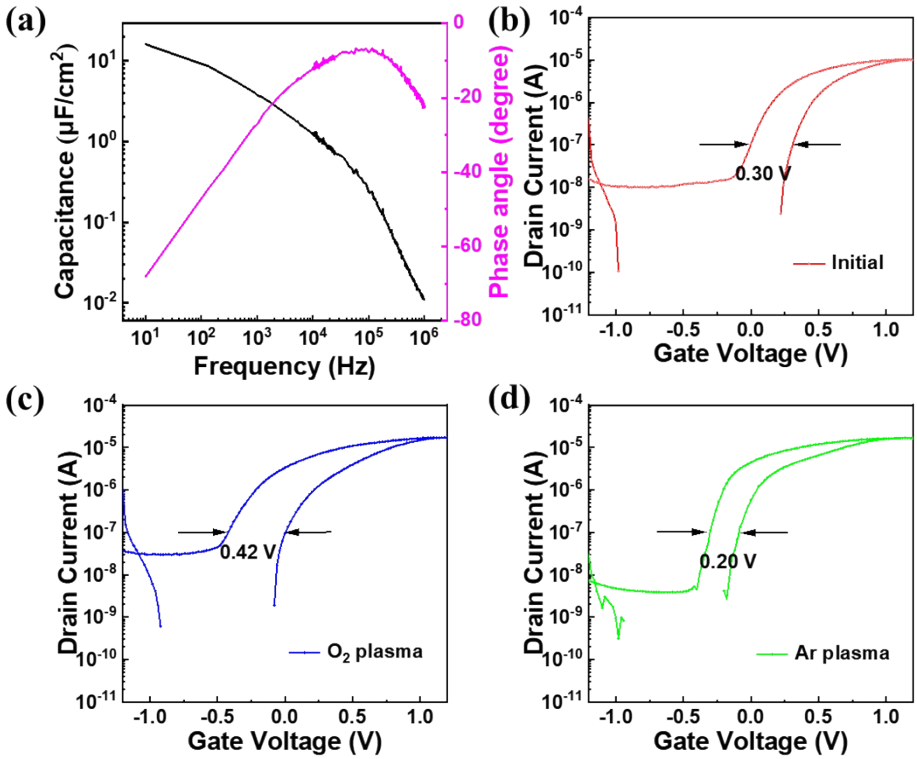

Fig. S1 (a) The capacitance–frequency curves and phase angle of $LiClO_4$/PVA ($LiClO_4$: PVA = 1:1) electrolyte. Transfer characteristic curves of ITZO EGTs subjected to plasma treatments: (b) Initial, (c) O_2 plasma, and (d) Ar plasma.

Table S1 The deposition rate of sputtered particles under different λ values.

λ^* (m)	0.34	0.67	1.34
Gas pressure (Pa)	1.6	0.8	0.4
Deposition rate (nm/s)	0.054	0.074	0.089

$\lambda^* = \frac{kT}{\sqrt{2}P\pi d^2}$, where P is the sputtering pressure, πd^2 is the collisional cross section, k is the Boltzmann constant, and T is the absolute temperature.

The sputtering power and Ar/O_2 flow ratio were fixed at 100 W and 60/3 sccm, respectively.

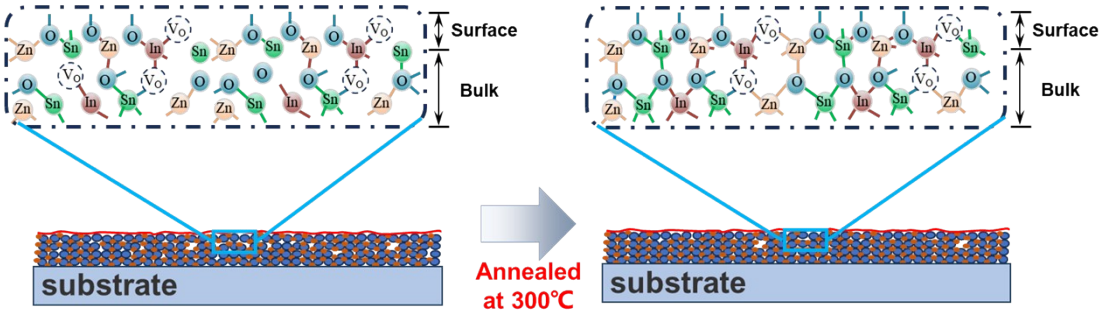

Fig. S2 Schematic of ITZO films subjected to a high-temperature thermal treatment.

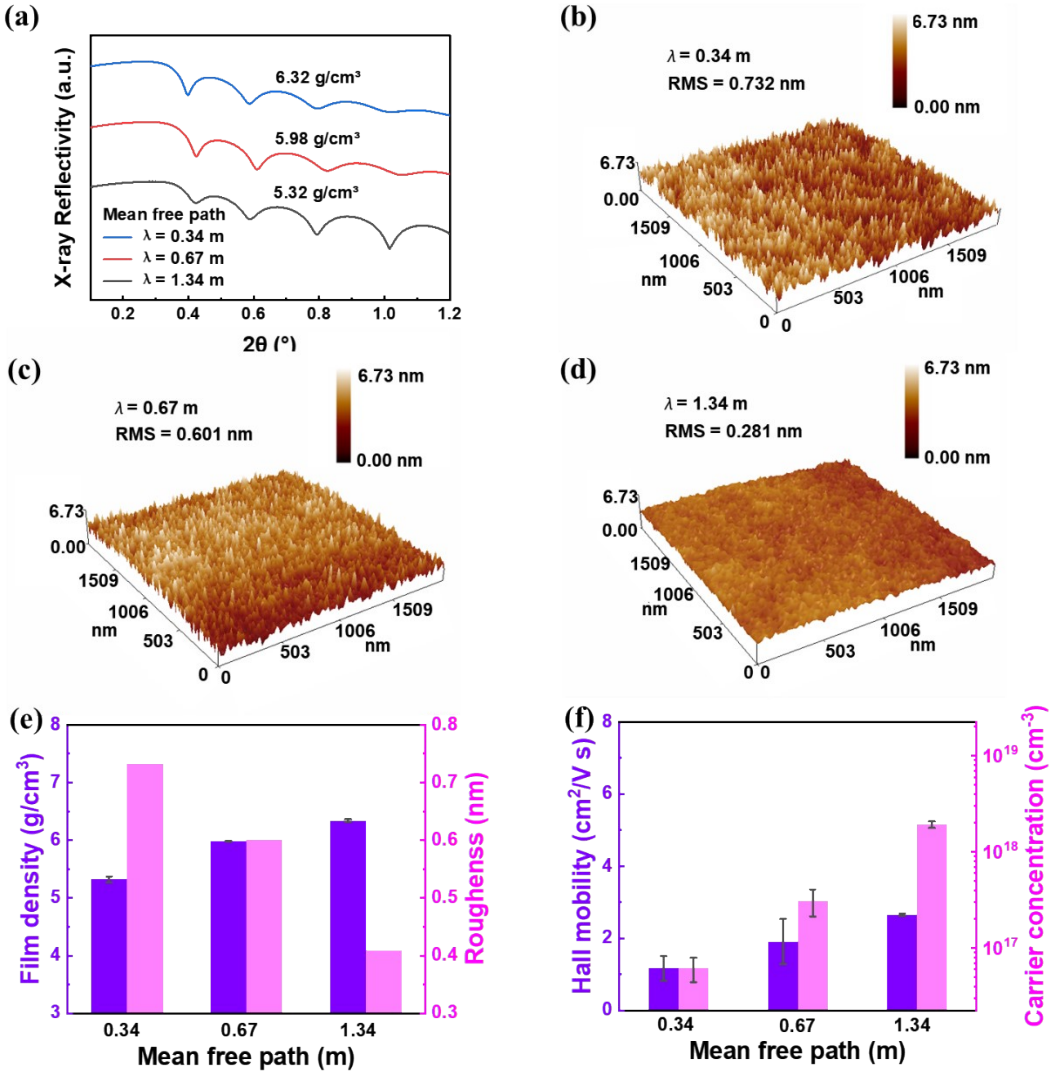

Fig. S3 (a) The density of ITZO films with different λ values. The surface morphology of ITZO films deposited at different λ values: (b) 0.34 m, (c) 0.67 m and (d) 1.34 m. Comparison of the properties of ITZO films with different λ values: (e) film density and roughness, (f) Hall mobility and carrier concentration.

Table S2 The deposition rate of sputtered particles under different ρ values.

ρ* (mg/m^3)	6.30	6.34	6.41
Ar/O_2 flow ratio (sccm)	60/6	60/3	60/0
Deposition rate (nm/s)	0.081	0.089	0.128

* $\rho = \frac{n\bar{M}}{V}$, where $\bar{M}$ is the mean molar mass of sputtering gas, V is the volume of sputtering gas, n is the amount of substance of sputtering gas.

The sputtering power and P were fixed at 100 W and 0.4 Pa, respectively.

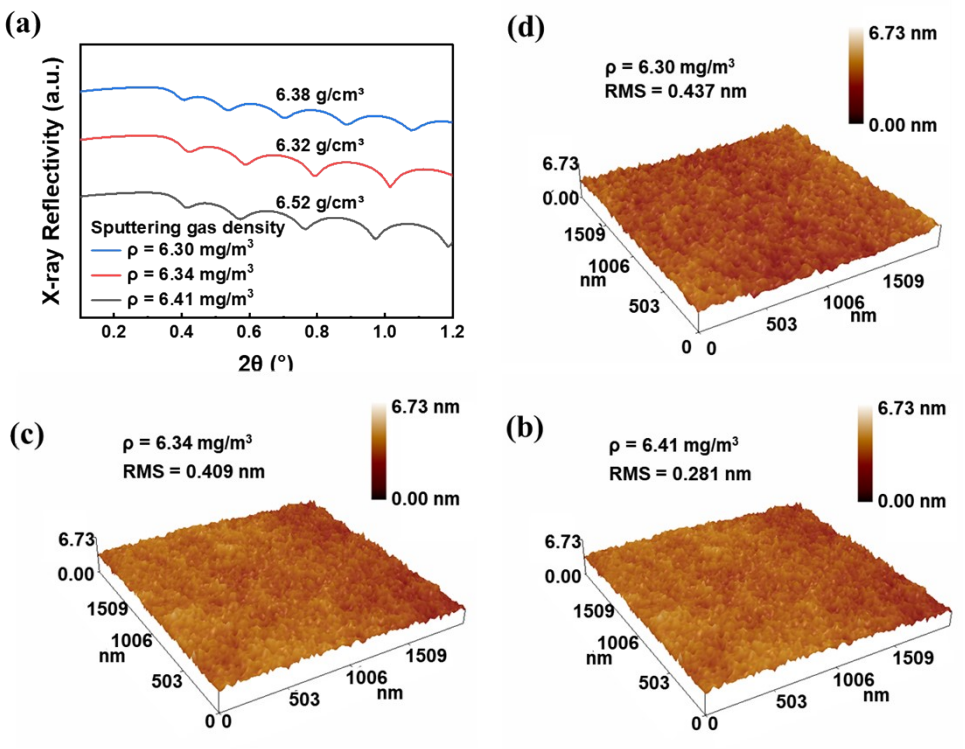

Fig. S4 (a) The density of ITZO films with different ρ values. The surface morphology of ITZO films deposited at different ρ values: (b) 6.30 mg/m^3, (c) 6.34 mg/m^3 and (d) 6.41 mg/m^3.

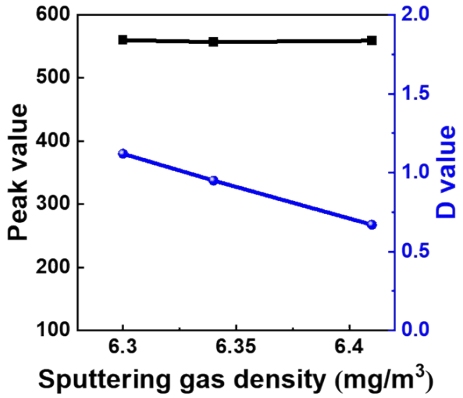

Fig. S5 The peak and D values as a function of the ρ values.

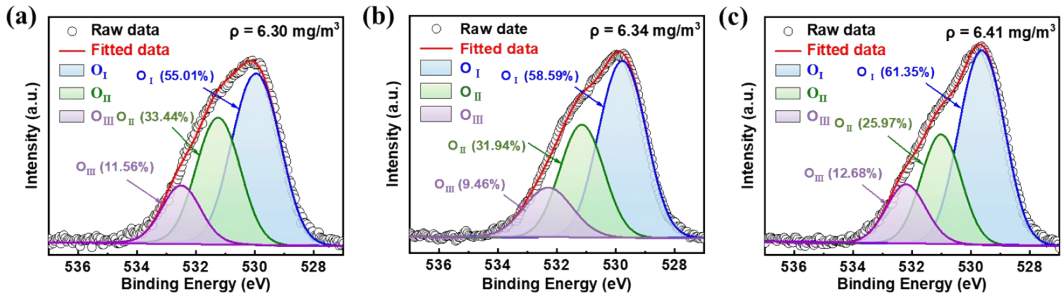

Fig. S6 The O1s spectra of ITZO thin films with different ρ values: (a) 6.30 mg/m^3, (b) 6.34 mg/m^3, (c) 6.41 mg/m^3. (O_I: 529.80 ± 0.20 eV, O_{II}: 531.30 ± 0.10 eV, and O_{III}: 532.35 ± 0.15 eV)

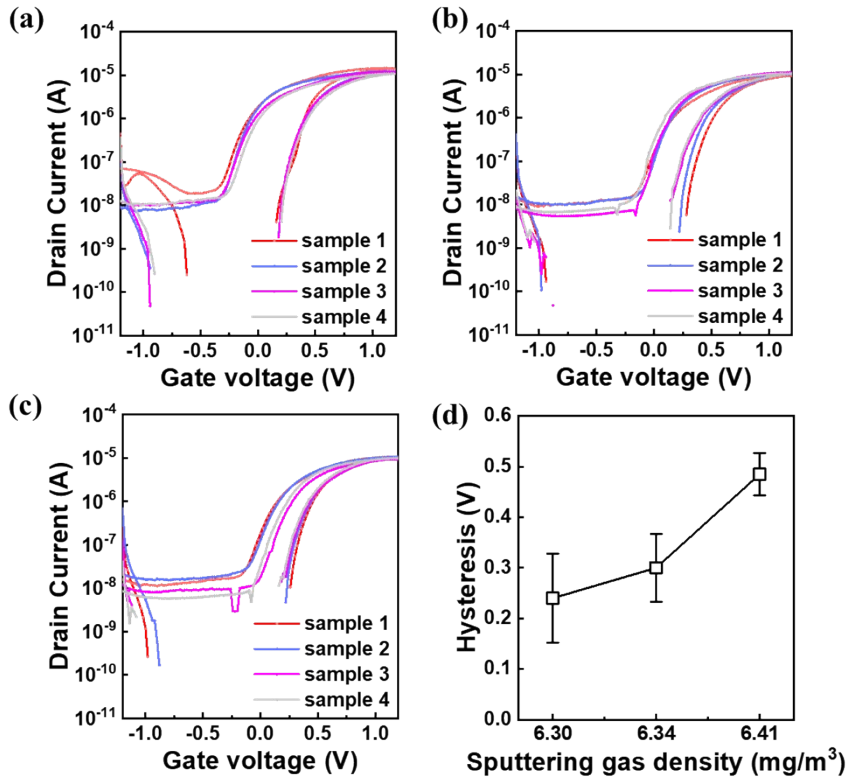

Fig. S7 The transfer characteristic curves of EGTs based on a-ITZO films deposited at different ρ values: (a) 6.30 mg/m^3, (b) 6.34 mg/m^3, (c) 6.41 mg/m^3. (d) The hysteresis width of ITZO EGTs.

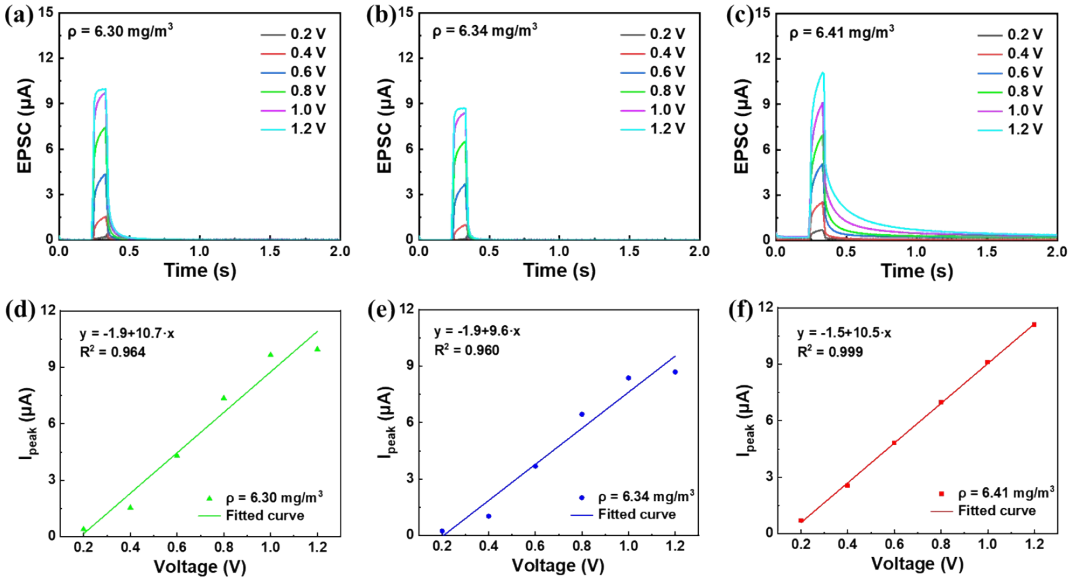

Fig. S8 The EPSC triggered by pulsed gate voltage with different amplitudes for ITZO EGTs under different ρ values: (a) 6.30 g/m^3, (b) 6.34 g/m^3, (c) 6.41 g/m^3.

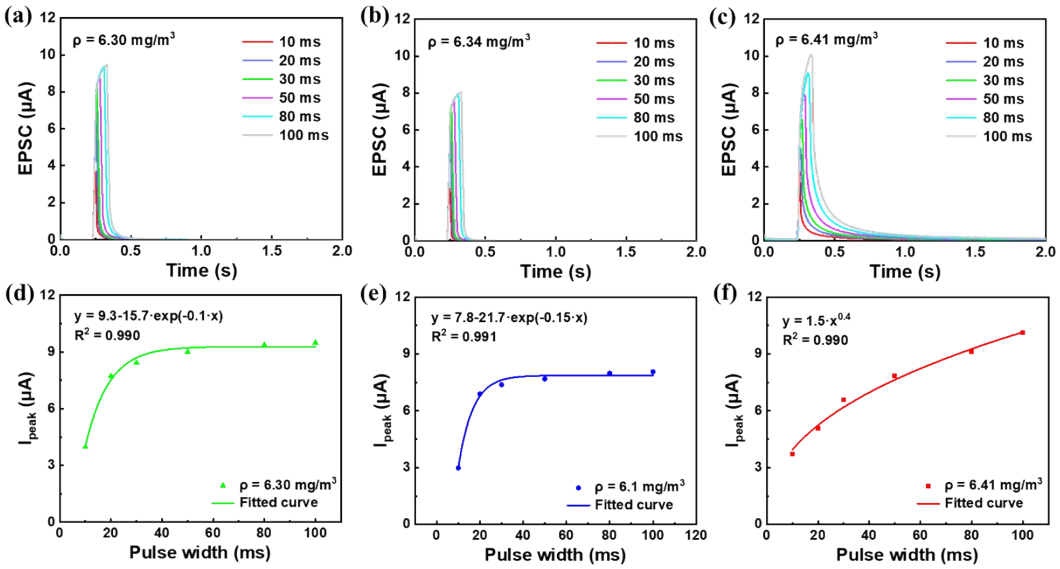

Fig. S9 The EPSC triggered by pulsed gate voltage with different durations for ITZO EGTs under different ρ values: (a) 6.30 g/m^3, (b) 6.34 g/m^3, (c) 6.41 g/m^3.

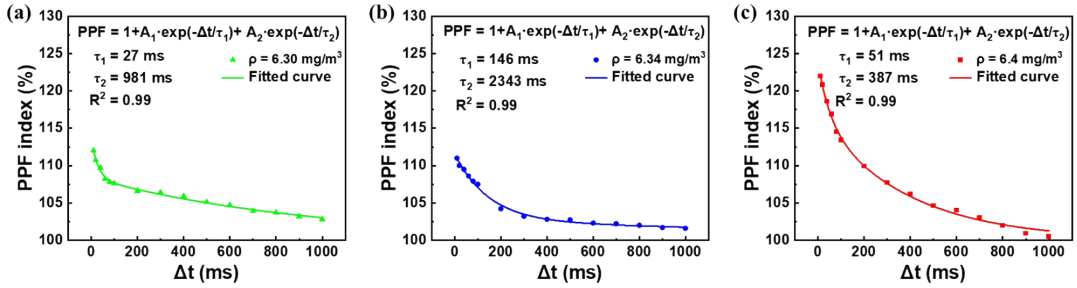

Fig. S10 Dependence of PPF index on pulse interval time (Δt) in ITZO EGTs equipped ITZO films deposited at different ρ values: (a) 6.30 g/m^3, (b) 6.34 g/m^3, (c) 6.41 g/m^3.

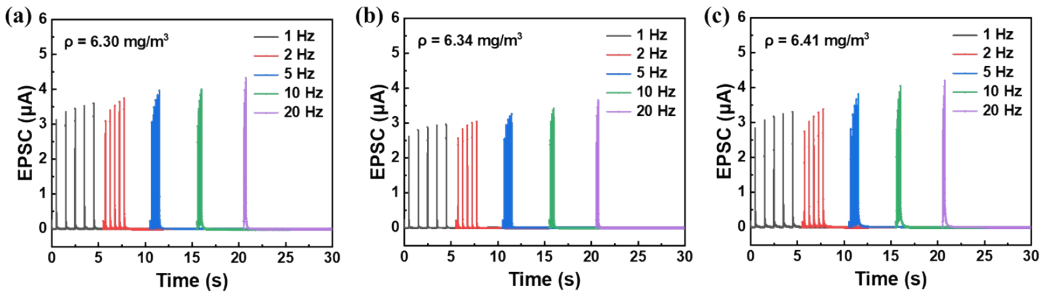

Fig. S11 The EPSC response to five consecutive pulses with different pulse frequencies for ITZO EGTs equipped ITZO films deposited at different ρ values: (a) 6.30 g/m^3, (b) 6.34 g/m^3, (c) 6.41 g/m^3.

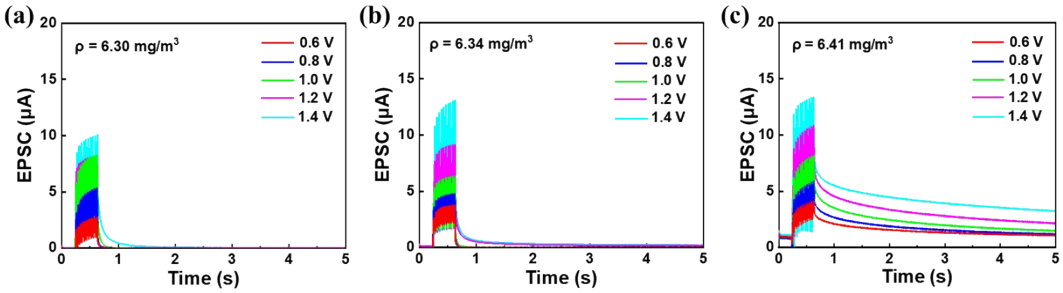

Fig. S12 EPSC triggered by multiple pulses with different amplitudes (V_{DS} =0.1 V) for ITZO EGTs equipped ITZO films deposited at different ρ values: (a) 6.30 g/m^3, (b) 6.34 g/m^3, (c) 6.41 g/m^3.

Table S3 Performance comparison of different oxide EGTs

Device	Linearity	# of weights	Max/min weight ratio	Operation condition	Accuracy	Ref
Li-PVA/ITZO	0.89/-1.10	40	17.73	±1.5 V	91%	This work
Li-PEO/ZnO	0.21/-0.12	32	——	±5.0 V	10.01%	[1]
Na-PEO/ZnO	0.45/-0.4	32	——	±5.0 V	87.73%	[1]
K-PEO/ZnO	0.53/-0.41	32	——	±5.0 V	87.96%	[1]
Li-PFOTS5/ZnO	-1.21/0.83	60	13.51	±4.0 V	89.71%	[2]
CdSe/IGZO	0.32/-1.37	20	——	±5.0 V	90.10%	[3]
LATP/IGZO	1.04/−2.22	50	——	±20.0 V	94.80%	[4]
Li-PEO/InZnO	4.97/-4.55	——	1.79	±1.0 V	≈87.50%	[5]
ZBO-In_2O_3	0.85/-2.66	20	6.26	-2V-4V	93.80%	[6]
Li-PEO	——	40	15	0-6V	91.60%	[7]
Li-ZnO		100			85.00%	[8]

(1) Lee H, Cho J, Jin M, et al. Electrochemical analysis of ion effects on electrolyte-gated synaptic transistor characteristics[J]. ACS nano, 2024, 18(7): 5383-5395.

(2) Jin M, Lee H, Im C, et al. Interfacial ion-trapping electrolyte-gated transistors for high-fidelity neuromorphic computing[J]. Advanced Functional Materials, 2022, 32(24): 2201048.

(3) Kwon S M, Kang S H, Cho S S, et al. Bidirectionally modulated synaptic plasticity with optically tunable ionic electrolyte transistors[J]. ACS Applied Electronic Materials, 2022, 4(6): 2629-2635.

(4) Park J M, Hwang H, Song M S, et al. All-solid-state synaptic transistors with lithium-ion-based electrolytes for linear weight mapping and update in neuromorphic computing systems[J]. ACS applied materials & interfaces, 2023, 15(40): 47229-47237.

(5) Cong H, Chang Y, Zhou R, et al. Rational tuning of the cation ratio in metal oxide semiconductor nanofibers for low-power neuromorphic transistors[J]. Science China Materials, 2023, 66(8): 3251-3260.

(6) Guo Y, Wu F, Dun G H, et al. Electrospun Nanofiber-Based Synaptic Transistor with Tunable Plasticity for Neuromorphic Computing[J]. Advanced Functional Materials, 2023, 33(5): 2208055.

(7) Liu C, Shen X, Fan S, et al. Synaptic characteristics and neuromorphic computing enabled by oxygen vacancy migration based on porous In_2O_3 electrolyte-gated transistors[J]. ACS Applied Electronic Materials, 2023, 5(8): 4657-4666.

(8) Guo Y, Wu F, Dun G H, et al. Electrospun Nanofiber-Based Synaptic Transistor with Tunable Plasticity for Neuromorphic Computing[J]. Advanced Functional Materials, 2023, 33(5): 2208055.